Carbohydrate Polymers 79 (2010) 989–997

Contents lists available at ScienceDirect

Carbohydrate Polymers

journal homepage: www.elsevier.com/locate/carbpol

Novel preparation and characterization of porous alginate films

Xiaoliang Wang [a,1], Xiang Li [a], Eleanor Stride [a], Jie Huang [a], Mohan Edirisinghe [a,*], Carl Schroeder [b], Serena Best [b], Ruth Cameron [b], Debbie Waller [c], Athene Donald [c]

[a] Department of Mechanical Engineering, University College London, Torrington Place, London WC1E 7JE, UK
[b] Department of Materials Science & Metallurgy, University of Cambridge, Pembroke Street, Cambridge CB2 3QZ, UK
[c] Cavendish Laboratory, University of Cambridge, JJ Thomson Avenue, Cambridge CB3 0HE, UK

ARTICLE INFO

Article history:
Received 16 July 2009
Received in revised form 1 October 2009
Accepted 13 October 2009
Available online 17 October 2009

Keywords:
Alginate
Film
Porosity
Bubble
Structure

ABSTRACT

Porous alginate films were prepared using a novel route in which alginate solutions of similar surface tensions but different viscosities were bubbled using a T-junction device to generate the films. The relationship between bubble size and bubbling conditions such as solution flow rate and air pressure was systematically investigated. The films obtained were characterized by optical microscopy, combined focused ion beam/scanning electron microscopy, and ultrasound reflection measurements. It is concluded that in a film, the thickness can be varied from 1–40 μm, where the minimum and maximum represent bubble-free and bubble-containing areas, respectively. Based on the characterization results obtained, a possible structure for the bubbles in the films is hypothesized.

© 2009 Elsevier Ltd. All rights reserved.

1. Introduction

Naturally derived polysaccharides such as chitosan, alginate and hyaluronic acid are widely used in biomedical engineering. Extensive attention has been focused on utilizing such natural materials in drug, enzyme or protein delivery (Jameela, Misra, & Jayakrishnan, 1994; Wang, Ye, Dai, Liu, & Tong, 2007), wound dressings, as well as scaffolds for tissue engineering (Mjahed, Porcel, Senger, et al., 2008). Whether in the form of microspheres, multilayer films or scaffolds, their polyelectrolytic and hydrophilic properties make them excellent protective matrices for small bioactive molecules such as BSA, insulin or other growth factors as well as cells (Zhang, Cai, Bei, & Wang, 2004). Therefore, controlled processing of these polymeric materials is of great importance, aiming at fabrication of specifically designed surfaces and interior structures. Many conventional processing techniques, involving the use of organic solvents or harsh conditions, are not suitable to process natural polymers, because the product cannot preserve the inherent cell-affinity of these polymers.

A range of microfluidic devices has been used to prepare micro-scale structures from advanced materials (Tan & Takeuchi, 2007). Based on flow regulation from ultra-thin capillaries or a specific orifice, microfluidic devices are capable of generating near-monodisperse structures such as microbeads, microcapsules and microbubbles (Ganan-Calvo & Gordillo, 2001; Okushima, Nisisako, Torii, & Higuchi, 2004; Pancholi, Farook, Moaleji, Stride, & Edirisinghe, 2008a; Talu, Lozano, Powell, Dayton, & Longo, 2006). Of these different microfluidic techniques, an air pressure-driven T-junction microbubbling device provides an efficient, practical and economical way to generate monodisperse microbubbles from polymer solutions or suspensions (Pancholi et al., 2008a). Phospholipid-coated microbubbles with polydispersivity in the range of ±1% have been successfully prepared using a T-junction device, where separate columns of liquid and gas meet at a junction, the gas is encapsulated by the liquid and bubbles are pinched off in quick succession. Microbubble preparation using a T-junction microfluidic device offers many advantages. For instance, the operational control of pressure and flow rate conditions is easily achieved and thus the formation of microbubbles is reproducible. The microbubble size can be varied by controlling the gas pressure/flow rate ratio as well as the capillary diameter. Furthermore, within certain limits, microbubble yield can be increased by increasing the fluid flow rates. Due to the fact that the T-junction microfluidic device ensures the monodispersity of microbubbles, it is very promising for incorporating some functionalized nanoparticles onto the surface of microbubbles (Stride & Edirisinghe, 2008). Also, the T-junction microbubbling technique can be combined with other processing techniques such as electrohydrodynamic atomization to further vary bubble characteristics, in particular size and size distribution (Pancholi, Stride, & Edirisinghe, 2008b).

* Corresponding author.
E-mail address: m.edirisinghe@ucl.ac.uk (M. Edirisinghe).
[1] Permanent address: National Engineering Research Center for Biomaterials, Sichuan University, Chengdu 610064, PR China.

0144-8617/$ - see front matter © 2009 Elsevier Ltd. All rights reserved.
doi:10.1016/j.carbpol.2009.10.025

Alginate, which is an anionic biopolymer originating from seaweed, is of widespread interest on account of its rapid ionic induced gel formation process, which can be achieved without involving any organic solvents. In this study, alginate has been chosen as the model polymer to be processed by using a T-junction microbubbling device with the aid of a surfactant (polyethyleneglycol 40-stearate). Polyethyleneglycol 40 stearate (PEG-40S) is a non-ionic surfactant, which is increasingly used in pharmaceutical preparations and delivery systems (Jiao, 2008). It consists of polar and non-polar segments in its molecular structure. The combination of a hydrophilic "head" and lipophilic "tail" produces a range of interfacial activity and versatile functions such as those of emulsifiers, surface modification agents and solubilizers. PEG-40S has also been chosen as the surfactant in fabricating lipid-coated monodispersed microbubbles in many instances (Borden & Longo, 2002; Klibanov, Rychak, Yang, et al., 2006; Pancholi et al., 2008b).

In this study, a range of alginate films containing microbubbles in a variety of different arrangements were prepared using a T-junction device. The films were studied using microscopy, focused ion beam/scanning electron microscopy (FIB/SEM) and ultrasound reflection measurements to characterize the wide variety of pore structures present in the films prepared.

2. Experimental details

2.1. Materials and solution preparation

2.1.1. Preparation of alginate–surfactant system (System A)

The surfactant PEG-40S (Sigma–Aldrich, Poole, UK, density 1300 kg/m^3) was dissolved in deionized water and stirred for approximately 1 h with a magnetic stirrer; this was followed by the addition of sodium alginate powder (low viscosity, Sigma–Aldrich, Poole, UK) to the solution which was done slowly to ensure complete dissolution. Three alginate solutions were prepared with the concentration of alginate set at 7.5, 10 and 12.5 mg/ml. The concentration of surfactant PEG-40S in all the solutions (System A) was kept constant at 10 mg/ml.

2.1.2. Preparation of phospholipid–alginate–surfactant system (System B)

Phospholipid (0.1% w/w) was added to prepare System B by dispersing L-α-phosphatidylcholine (hydrogenated, Type I-EH, Sigma) into deionized water firstly, and then PEG-40S and alginate were added to the suspension, in succession as in System A. The concentration of alginate and surfactant in this suspension were fixed at 10 mg/ml. The suspension was stirred for 3 h to ensure good dispersion. This system was further dispersed by using an ultrasonic disrupter (Branson Sonifier 250; set at 7 W for 120 s, then 12 W for 30 s) before bubbling. "System B-1" refers to the suspension which was heated to 50 °C before microbubbling. Heating, which obviously decreases viscosity, is expected to result in better alignment of the microbubbles in the final structure.

2.1.3. Characterization of solutions

The viscosity of the solutions was measured using a "viscoeasy" rotational viscometer (Camlab Ltd., Cambridge, UK) working at a shear rate of 100 rpm. The surface tension was measured with a Kruss Tensiometer (Model-K9, Kruss GmbH, Germany) using the plate method. All measurements were carried out at the ambient temperature (~20 °C) and the mean values of six readings were taken to ensure repeatability. Both viscosity and surface tension equipment were calibrated with ethanol prior to use.

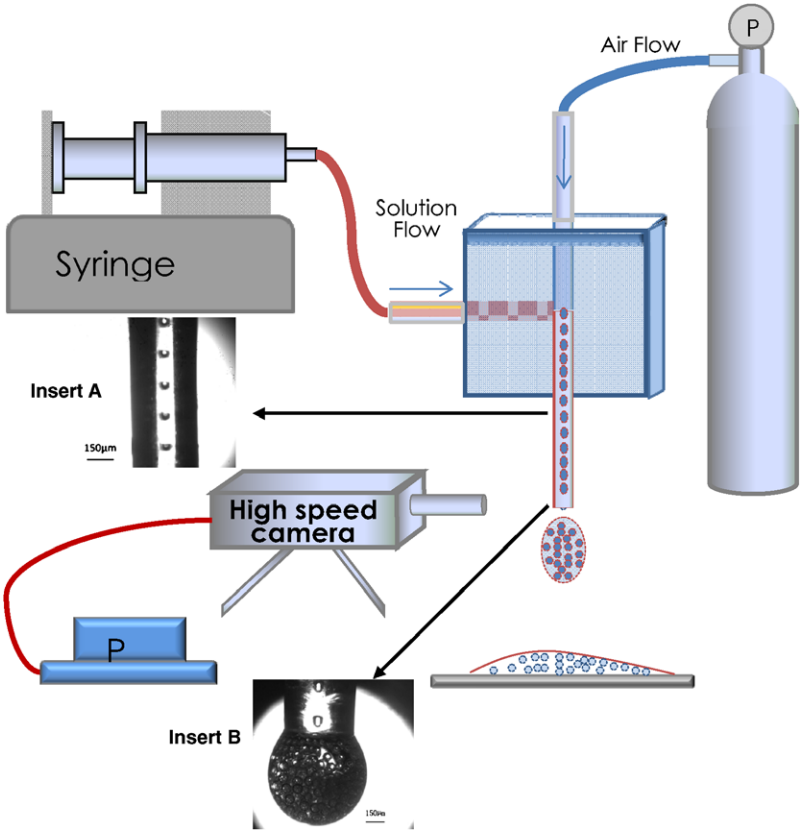

Fig. 1. Schematic diagram of T-junction microbubbling device. Inserts A and B show actual high-speed camera clips of the process.

Table 1
Properties of the solutions, digits after System indicate alginate concentration in mg/ml.

Sample	Viscosity/mPa s	Surface tension/mNm^{-1}
System A-7.5	21 ± 0.3	48 ± 0.6
System A-10	32 ± 0.5	48 ± 0.3
System A-12.5	50 ± 0.2	51 ± 0.5
System B	32 ± 0.5	49 ± 0.4
System B-1	30 ± 0.4	51 ± 0.1

2.2. Preparation of films

The T-junction microbubbling device used has been described in detail before (Pancholi et al., 2008a). In brief, as indicated in Fig. 1, two capillaries with internal diameter 150 μm were aligned and fixed within a rigid polymer block. The two capillaries were separated by a distance of 70 μm. A third tube, also of the same diameter, was inserted perpendicularly into the polymer block to form the T-junction. All the capillaries were fixed securely within the polymer block and the unit was designed to withstand the high pressure generated during the microbubbling process. Air at a controlled pressure was introduced into the device by a gas cylinder through the top capillary whereas the perpendicular capillary was connected to a 20 ml stainless steel syringe (KD Scientific, Holliston, MA, USA).

The liquid flow rate and the air pressure could be easily controlled by a syringe pump (Harvard, PHD 4400) and a pressure gauge, respectively. When the alginate solution was introduced to the T-junction at a constant flow rate, the air pressure was increased to prevent the upstream movement of the solution. When the air pressure was high enough to overcome the surface tension of the solution, a gas ligament surrounded by liquid was formed in the capillary and stable microbubbling was established. Images of the microbubbles were captured using a Phantom V5 high-speed camera (Vision Research Ltd., Bedford, UK). Microbubbles generated were collected on glass slides at the outlet of the capillary.

All three solutions of System A were bubbled at a constant liquid flow rate of 100 μl/min. The effect of different flow rates (100, 200, 400 μl/min) on microbubbling was also investigated. Microbubbles were collected on glass slides and examined by optical microscopy (Nikon Eclipse ME 600) immediately. Micrographs of different areas were taken and the diameters of 100 microbubbles were measured for each set of conditions to calculate the average diameter using Image Pro-Express software (Version 5.0).

The procedure for fabricating porous alginate films was based on the understanding gained in the microbubbling experiments. The liquid flow rate was kept constant at 200 μl/min. The air pressure was set at 80 kPa and 83 kPa for System A and System B, respectively, unless otherwise stated. About 50 μl of liquid containing microbubbles was collected on a glass slide at the outlet

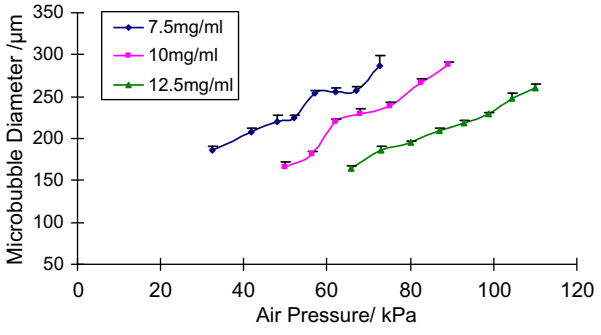

Fig. 2. Relationship between the microbubble diameter and the air pressure in System A for different solution concentrations, liquid flow rate is 100 μl/min.

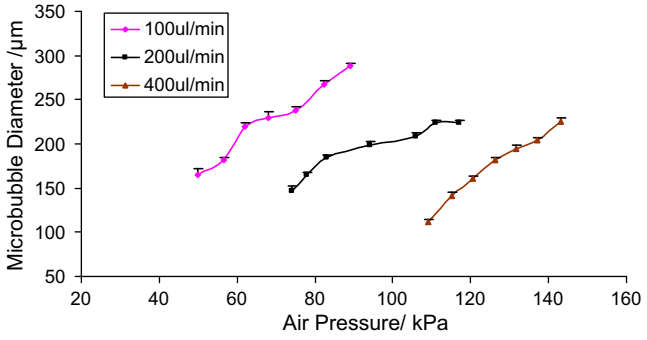

Fig. 3. Relationship between microbubble diameter and the air pressure in System A at different liquid flow rates, concentration of alginate is 10 mg/ml.

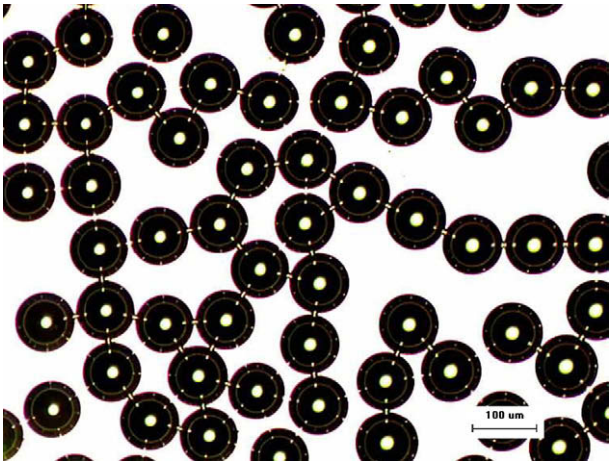

Fig. 4. Optical micrograph of the smallest diameter microbubbles generated in this work. System A with 12.5 mg/ml alginate, liquid flow rate 400 μl/min, air pressure 148 kPa.

of the T-junction device under these conditions. Subsequently, this slide with microbubbles on it was turned over to cover a second glass slide coated with 0.2 M $CaCl_2$ solution. A thin layer of gel containing microbubbles was formed and was further crosslinked by immersing in 0.2 M $CaCl_2$ solution. At different time points such as 0.5 h, 24 h, the bubbly gels were taken out and placed on glass slides to be air-dried. All the dry samples were then rinsed with deionized water to remove the excessive cross-linker and air-dried again. The films produced in this way were stored on glass slides at ambient temperature.

2.3. Characterization of films

2.3.1. Microscopy

To characterize the films, both optical microscopy (Zeiss Axiotech microscope fitted with a digital camera) and scanning electron microscopy were used primarily to study the overall porous microstructure, but also to assess the cross-sections of thin films. Some samples for optical microscopy were viewed after being mounted under a No. 1 glass coverslip to give sharper images. Films were also studied using scanning electron microscopy (SEM, JEOL-LV 5500) and field emission SEM (JEOL JSM/6301F). In the case of SEM (JEOL-LV 5500), the secondary electron imaging mode was used. Details of the accelerating voltage (HV) and working distance (WD) are included with each relevant figure. The influence of the crosslinking period on the bubble evolution was investigated by field emission SEM, here the samples were sputter coated using carbon for 120s prior to examination.

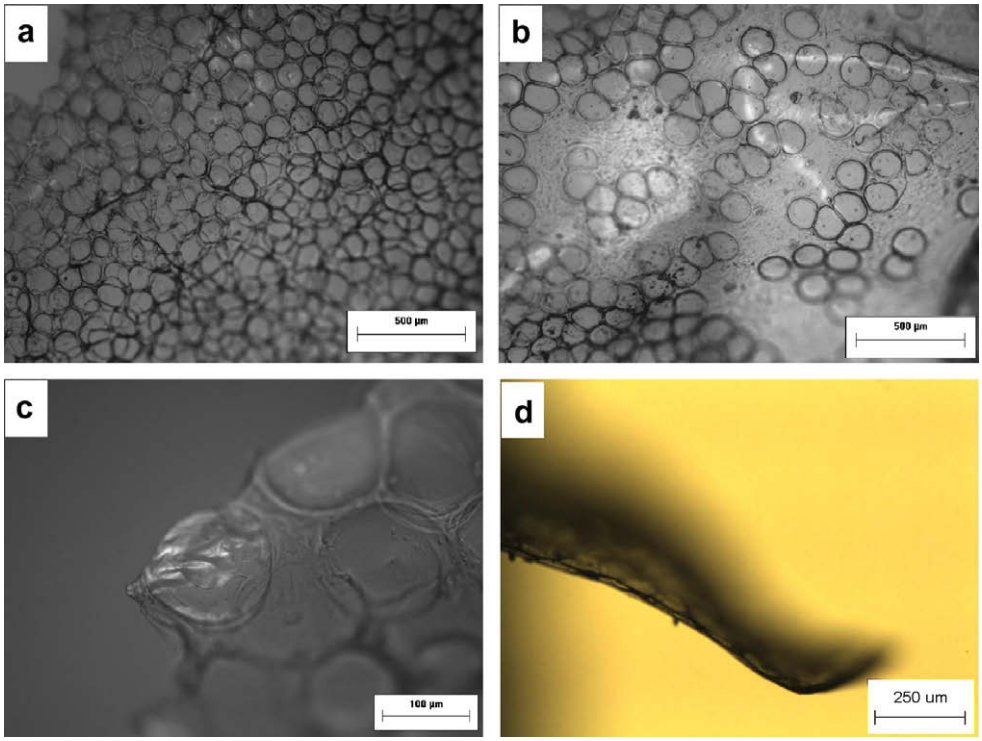

Fig. 5. Optical images of porous film from System A containing high (a) and low (b) bubble density areas, film fracture surface (c), and the cross-section (d).

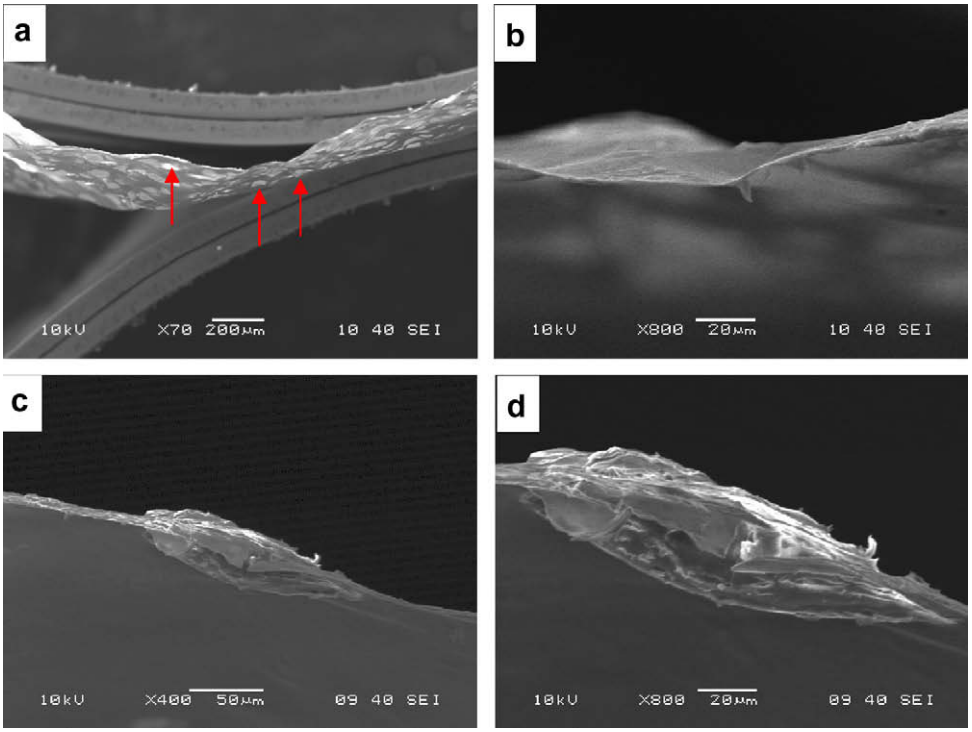

Fig. 6. Scanning electron micrographs of different areas of the cross-section of film generated from System B-1((a) HV 10 kV; WD 100 mm; (b) HV 10 kV; WD 90 mm; (c) HV 10 kV; WD 120 mm; (d) HV 10 kV; WD 110 mm).

2.3.2. Combined focused ion beam/scanning electron microscopy

Combined focused ion beam/scanning electron microscopy (FIB/SEM, FEI Philips Dualbeam Quanta 3D/SEM, JEOL-LV 5500) was used to obtain detailed information on the film cross-sections. Prior to imaging, the samples were coated with a thin layer of gold (<100 nm) to protect the film from beam damage. In addition a 1 µm layer of platinum was applied to milling sites to improve the function of the milling beam and provide a clean milling surface. This process took place within the microscope itself, allowing flexibility in the selection of suitable site areas for milling.

2.3.3. Ultrasound reflectometry

Film samples were suspended in a bath of distilled water on a low density polyethylene membrane (~150 μm thick). The samples were insonified using a focused transducer having a nominal centre frequency of 15 MHz, diameter 10 mm and a focal length of 76.2 mm (Panametrics, Olympus NDT, Lancashire, UK) driven using a pulser/receiver unit (Panametrics 5072 PR, Olympus NDT, Lancashire, UK). The signals from the transducer were captured using a digital oscilloscope (LeCroy 9310 M Dual 300 MHz) connected to a PC containing purpose written signal processing software to detect the amplitude of the reflected signal from each sample.

3. Results and discussion

3.1. Materials and solution characteristics

The physical properties, in particular the surface tension and viscosity of the solutions which undergo microbubbling, are a major factor in determining whether using a T-junction to process these solutions is possible. Adding surfactants is an efficient way to adjust the surface tension and some studies have been carried out to investigate the interactions between alginate and surfactants (Jiao, 2008; Yang, Chen, & Fang, 2009). A relatively high concentration of PEG-40S (10 mg/ml) compared with other studies (1 mg/ml) (Borden & Longo, 2002) was necessary to reduce the surface tension in order to enable T-junction microbubbling. The surface tension and viscosity of each system is given in Table 1 which shows that with increasing concentration, alginate solutions become more viscous while the surface tension remains almost constant. The aim in incorporating phospholipids into the alginate–surfactant system was to coat the microbubbles with a protective thin layer which would inhibit gas diffusion but this did not seem to affect viscosity or surface tension.

3.2. Microbubbles

It is well-known that the liquid flow rate, air pressure and the liquid viscosity have a significant influence on bubble formation and the eventual size of bubbles in T-junction microbubbling (Pancholi, Stride, & Edirisinghe, 2008c). The general trend is that smaller bubbles can be produced with higher flow rates and higher viscosities. Results in Figs. 2 and 3 demonstrate these facts. When the liquid flow rate was set at 100 μl/min, the three solutions of System A were successfully processed to generate microbubbles. As shown in Fig. 2, microbubbles with different average diameters were obtained at different air pressures, with larger microbubbles being generated with increasing air pressure. This demonstrates that achieving a low air pressure/liquid flow rate ratio is crucial for generating bubbles with small average diameters. With increasing alginate concentration, the initial air pressure value, under which stable microbubbling was achieved, was also increased. The average diameters of the microbubbles prepared varied between 165 and 288 μm. All the samples had a polydispersity index (standard deviation/mean diameter) of 1–4%. It must be noted that by using finer capillaries, T-junction microbubbling can be used to generate much finer bubbles, whilst retaining near-monodispersivity (Pancholi et al., 2008b).

The influence of the liquid flow rate on the microbubble diameter (Fig. 3) showed that a higher initial air pressure was required to establish microbubbling at a higher liquid flow rate. Thus, a smaller bubble size was achieved whilst retaining the 1–4% polydispersity index. The smallest bubble diameter obtained in this study was 85 ± 4.5 μm (Fig. 4) using System A at an alginate concentration of 12.5 mg/ml with the liquid flow rate and the air pres-

Table 2
Samples from film forming experiments, a–l refer to Fig. 7.

Sample formulation	Crosslinking time/magnification			
	0.5 h		24 h	
	×50	×100	×50	×100
System A-10	a	b	c	d
System B	e	f	g	h
System B-1	i	j	k	l

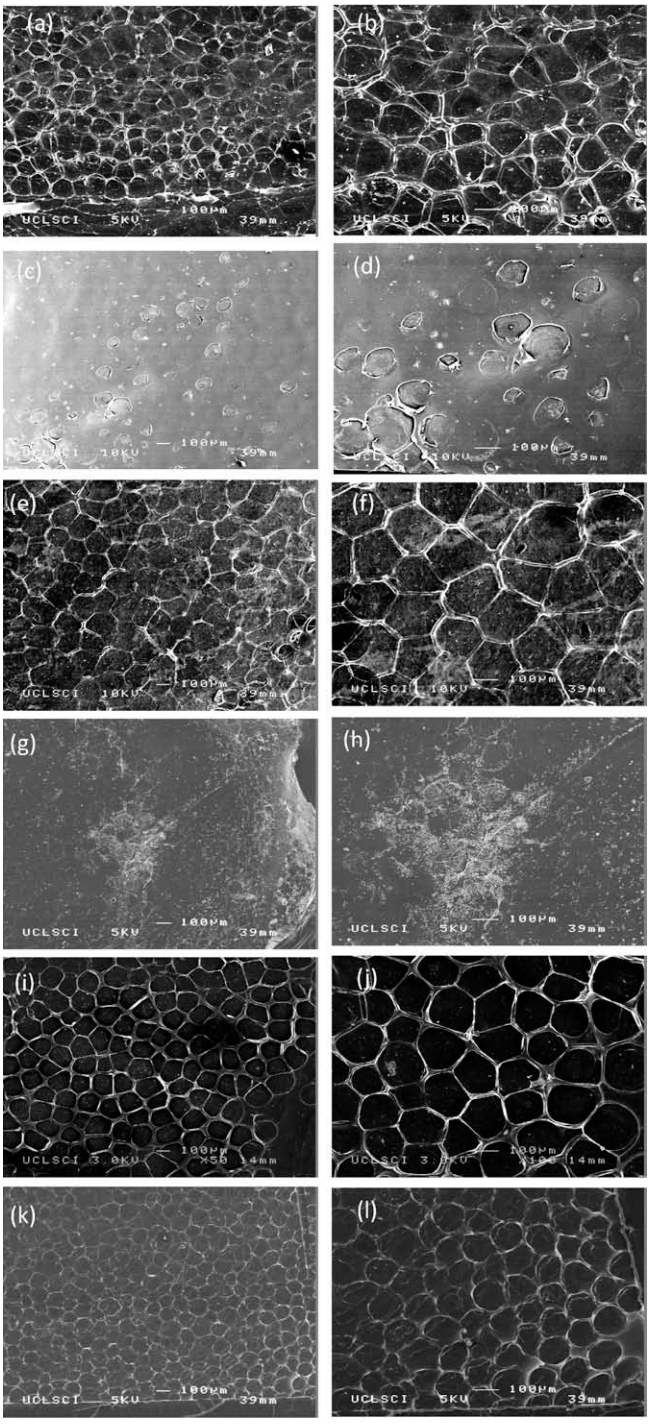

Fig. 7. Scanning electron micrographs of film surface, System A-10 (a–d), System B(e–h), System B-1(i–l), with details in Table 2.

sure set at 400 μl/min and 160 kPa, respectively. Increasing both viscosity and liquid flow rate contributed positively to the reduction of bubble size within the parameter range of this research.

3.3. Film characteristics

3.3.1. Morphology of bubble films

Films with porous structures were successfully prepared by crosslinking samples generated using System A, System B and System B-1. An alternative method of crosslinking is to add a calcium salt to the alginate during processing to cause controlled gelling. However, this may lead to the blocking of the T-junction feeder and outlet capillaries.

The initial studies were conducted on a sample from System A-10 by using optical microscopy to check the bubble structure and the overall appearance of the film. Areas of high (Fig. 5a) and low (Fig. 5b) bubble density were identified and the fracture surface (Fig. 5c), including through-fractured bubbles, was studied. Bubble density in the films depended on the initial alignment of bubbles in the liquid obtained at the outlet of T-junction device, which can be further controlled by optimizing the bubble-collecting conditions. Further optical microscopy was carried out to view the film in cross-section and gain more information on the thickness of the film and the through-thickness shape of the bubbles. Cross-sectional imaging proved difficult due to the natural curvature of the film. Fig. 5d shows that the bubbles are not spherical, but squashed in the through-thickness direction. The thickness of the bubble containing sections of the films was estimated to be in the range of 25–80 μm.

Further scanning electron microscopy was performed to build on the information revealed by Fig. 5d, to understand the cross-sectional structure of the film. A sectioned sample from System B-1 was prepared for imaging. The low magnification image (Fig. 6a) shows the edge of the film in focus. It clearly shows regular light-colored regions (labeled by arrows) in the film corresponding to the bubbles. This gives a good indication of the aspect ratio of the bubbles within the film. At higher magnification (Fig. 6b) the film thickness can be estimated as 1–5 μm. A significant feature observed in the films is shown in Figs. 6c and d. Here, the film edge analyzed was created by sectioning the original film with a scalpel into smaller samples; from the features size (~130 μm in length) it can be concluded that this is a bubble in cross-section, although a large amount of debris created during sectioning obscures the detail of the structure. The most significant information from the images relates to the thickness of the bubble itself (~40 μm) in comparison with the film around it (~5 μm). The bubble section appears to be thicker than the surrounding film, therefore although the bubbles lie within the film, they can have a depth greater than shown in Figs. 6a and b.

The effect of different crosslinking time on the bubble morphology change has been obtained by examining samples from the three systems (Table 2) using SEM. Without the aid of phospholipid, System A gives a random surface structure after air-drying (Fig. 7a and b) indicating that gas diffusion and bubble coalescence took place rather randomly in this system. It also indicates that the ability to retain air in the bubble shell of System A is poor. Therefore, after dipping the sample in crosslinker solution for 24 h, surface morphology changes were observed (Fig. 7c and d). Only a few

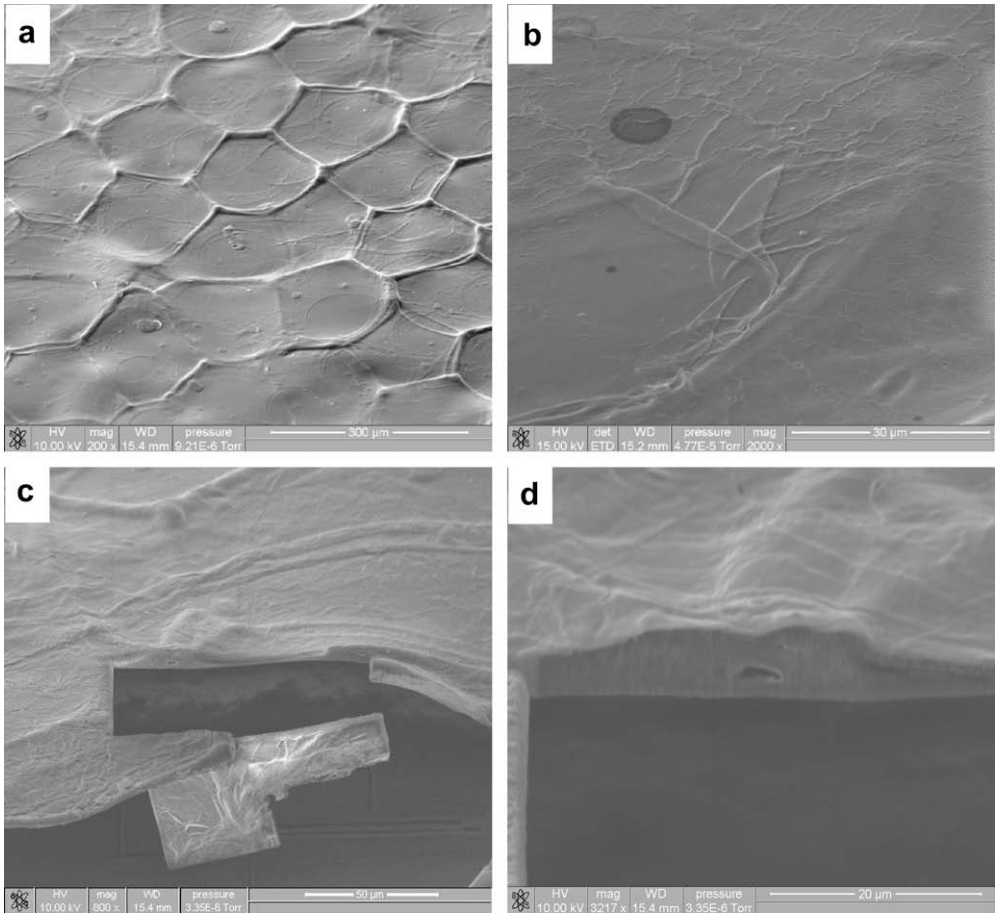

Fig. 8. FIB/SEM images of thin film from System A-10. (a) overview of surface; HV 10 kV; WD 154 mm (b) the bunching of material in central regions; HV 15 kV; WD 152 mm (c and d) milled cross-sections; HV 10 kV; WD 154 mm.

irregular bubbles were left on the film surface whilst the original boundaries of bubbles became unclear.

Lipid-coated monodisperse microbubbles possess enhanced stability when they are compared with those coated only with surfactant PEG 40-stearate. The amphiphilic nature of the phospholipid coating in such a combined system plays an important role in air retention (Talu et al., 2006). However, a regular bubble structure was not observed in System B, especially in the sample dipped in crosslinker solution for 24 h (Fig. 7g and h). This is likely to be due to the relatively small amount of phospholipid used as well as the influence of the presence of alginate macromolecules. The surface morphology of System B is more regular compared with System A, though the bubble stability needs to be further improved. It was found that heating of System B resulted in a uniform surface structure of the films prepared (System B-1). As shown in Fig. 7i–l in System B-1, a regular structure was achieved from samples crosslinked, for both 0.5 h and 24 h. The heating to 50 °C regulates the alginate molecular chain alignment (Wang et al., 2007), and the more defined chain arrangement achieved leads to more rigid bubbles, thus enhancing the stability of the structure during crosslinking and air-drying, leading to a better bubble structure in the films.

The FIB/SEM images helped to reveal more details of the microstructure in the films. Two film samples with different initial

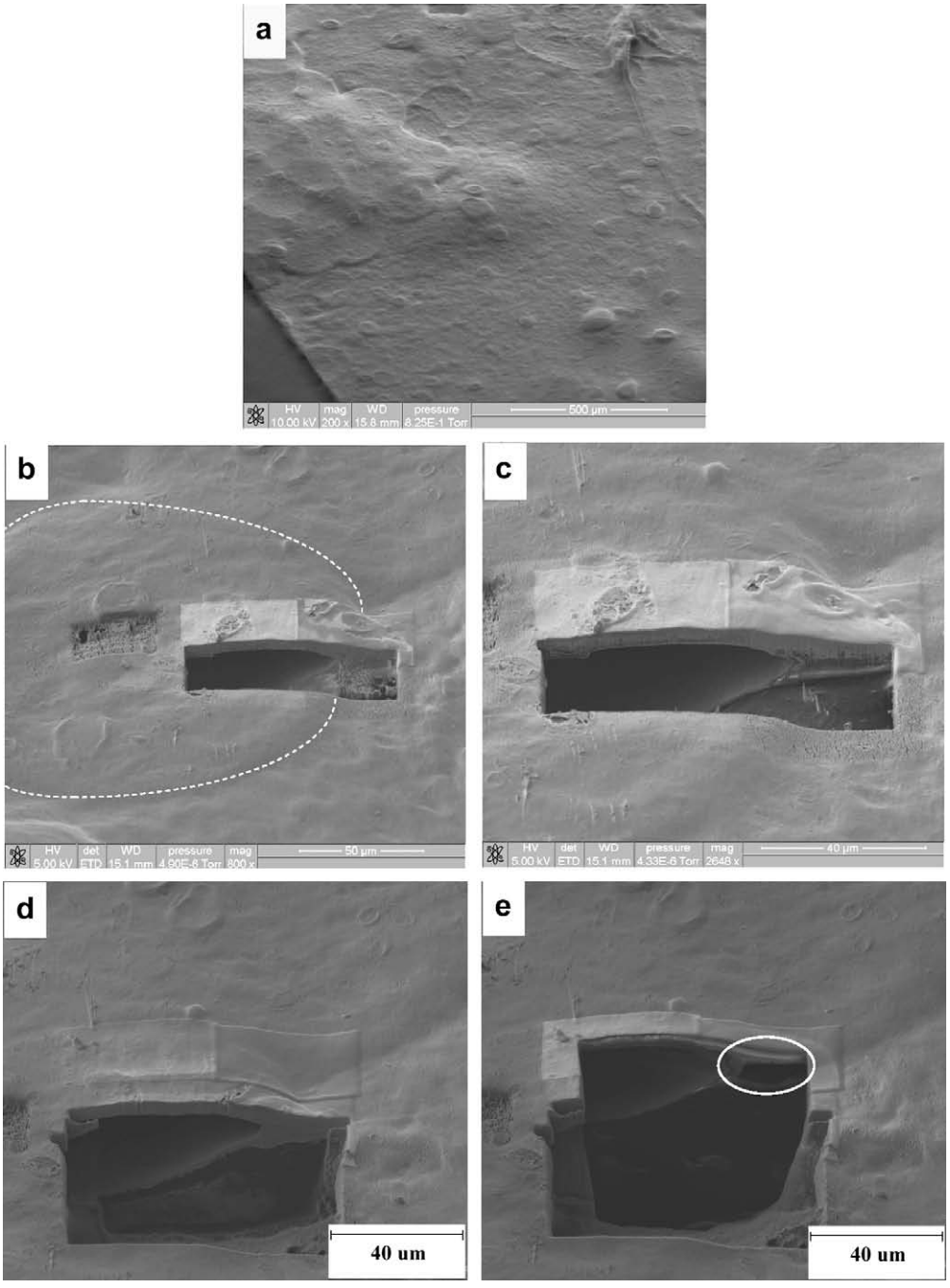

Fig. 9. FIB/SEM images of thin film from System B. (a) overview of surface; HV 10 kV; WD 158 mm. (b and c) details of milled cross-sections; HV 5 kV; WD 151 mm; dotted line in (b) – shows the outline of the bubble from the top surface. (d and e) start and end point of the cross-section of bubble edge; HV 10 kV; WD 151 mm; solid circle in (e) – shows highlights the area in which two bubbles are joined.

bubble size were prepared for FIB/SEM analysis. The first, with a larger initial bubble size (~180 μm), is from System A-10 (Fig. 8a–d); the other contains smaller sized bubbles (~130 μm) from System B (Fig. 9a–e). Fig. 8a clearly shows the bubble relics with ridges on the surface. This structure could imply that the bubbles in this sample have collapsed, leaving the thicker edges clearly discernable. This theory of bubble collapse is supported by higher magnification images, which clearly show bunching of excess material in the central region between the ridges (Fig. 8b). FIB milling results also supported this theory. FIB milling was carried out on the edge of the sample to reveal a through film thickness of <10 μm (Fig. 8c and d). Again, the lack of any significant bubble structure in cross-section is indicative of bubble collapse. The larger initial bubble size means that a larger air volume is present in the bubbles and this is the main reason for the collapse because it bears more intensive pressure when it is immersed in the cross-linker solution.

In contrast to the samples containing a larger bubble size, the fairly flat featureless surface (Fig. 9a) of the samples supporting a smaller bubble size, supplies further evidence to the suggested structural evolution of the bubbles. The aim of further FIB/SEM work on this sample was to concentrate on the prominent bubbles in the same way as above and explore their features. A well defined bubble with a diameter of ~150 μm was chosen, as highlighted in Figs. 9b and c, and a shallow section of 70 × 25 μm was milled at the edge. The resulting view clearly shows the structure at the edge of the bubble, as well as the upper and lower film surface. A series of slices were then made on the top edge of this section (Figs. 9d and e) to generate a 3D reconstruction of this area of the bubble. These consecutive sections show the curve at the edge of the bubble and the cavity of an adjacent bubble. Thus, the bubble edge becomes a separating wall between two distinct bubbles.

Overall, the bubbles in the films are not spherical like those in the liquid. Several reasons contributed to this. Firstly, the drying of the film changes bubbles morphology and, secondly, the compression applied between the two microscope slides force the bubble to flatten and attain a high aspect ratio. In addition, diffusion of air and the coalescence of the bubbles and wall collapse could also result in changes of bubble morphology.

3.3.2. Ultrasound reflectometry

The results from the ultrasound reflectometry measurements are shown in Fig. 10. As would be expected, the films containing smaller, more sparsely distributed pores produced smaller signals than those containing larger and/or more closely spaced ones. Similarly, the film containing well organized pore distributions from System A-10 produced the largest amplitude signals as would be predicted, since both the impedance contrast and proportion of energy scattered towards the transducer would have been maximized for this sample. There was not found to be a direct correlation between pore size and the amplitude of the reflected signal for all the samples and this is likely to be due to the fact that some films may have contained some interconnected pores and so liquid saturation would have reduced the reflected signal compared with what might have been expected for air filled cavities. These results thus demonstrate the potential for assessing pore size, distribution and sample saturation from ultrasound measurements. Accurate interpretation will require comparison with an appropriate model for scattering from porous media and this will be carried out in future work.

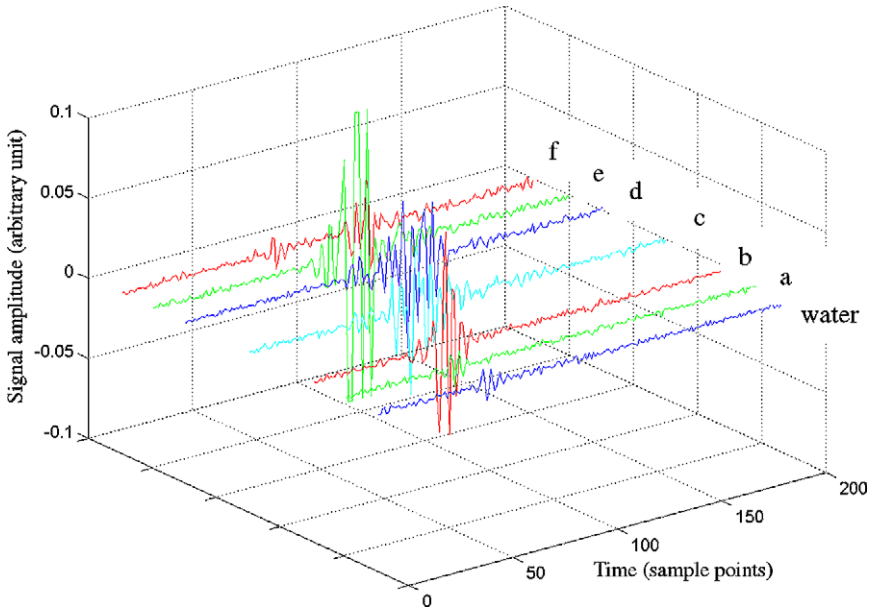

Fig. 10. Ultrasound reflectometry plots of porous films from System A-10(a, 0.5 h; b, 24 h), System B(c, 0.5 h; d, 24 h), System B-1(e, 0.5 h; f, 24 h).

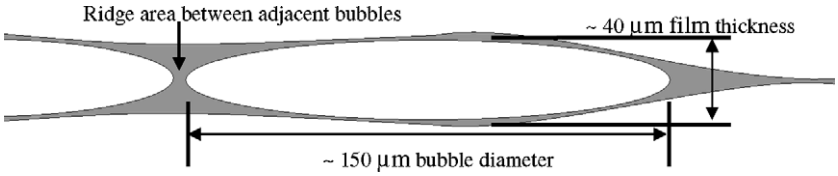

Fig. 11. Schematic diagram of hypothesized bubble structure.

4. Conclusions

A T-junction microbubbling device was successfully used to generate near-monodispersed alginate coated air-filled microbubbles. The relationship between microbubble size and the bubbling conditions has been systematically studied and optimized bubbling conditions give rise to films with bubbles size in the range of 80–290 μm. Bubbles were successfully incorporated in films and the use of phospholipid and pre-heating helped to improve air retention in alginate coated microbubbles. The combined FIB/SEM findings illustrate that there were two types of bubble-derived structures present in the films, namely bubble ridge relics structure and squashed-in bubble porous structure. The latter is hypothesized (Fig. 11) according to the characterization results, film thickness varies from ~1 μm in regions devoid of bubbles (usually towards the film edge) to ~40 μm when the bubble itself is incorporated into the total thickness.

Acknowledgements

The Chinese Scholarship Council, UCL Vinson Chu Scholarship Fund and Professor Xudong Li of Sichuan University are gratefully thanked for supporting Xiaoliang Wang's stay at UCL. EPSRC and BBSRC (Grant BB/E007422) are thanked for supporting the research of Carl Schroeder and Debbie Waller, respectively.

References

Borden, M. A., & Longo, M. L. (2002). Dissolution behavior of lipid monolayer-coated, air-filled microbubbles: effect of lipid hydrophobic chain length. *Langmuir, 18*, 9225–9233.

Ganan-Calvo, A. M., & Gordillo, J. M. (2001). Perfectly monodisperse microbubbling by capillary flow focusing. *Physical Review Letters, 87*, 274501/1–274501/4.

Jameela, S. R., Misra, A., & Jayakrishnan, A. (1994). Cross-linked chitosan microspheres as carriers for prolonged delivery of macromolecular drugs. *Journal of Biomaterials Science Polymer Edition, 6*, 621–632.

Jiao, J. (2008). Polyoxyethylated nonionic surfactants and their applications in topical ocular drug delivery. *Advanced Drug Delivery Reviews, 60*, 1663–1673.

Klibanov, A. L., Rychak, J. J., Yang, W. C., et al. (2006). Targeted ultrasound agent for molecular imaging of inflammation in high-shear flow. *Contrast Media & Molecular Imaging, 1*, 259–266.

Mjahed, H., Porcel, C., Senger, B., et al. (2008). Micro-stratified architectures based on successive stacking of alginate gel layers and poly(ι-lysine)-hyaluronic acid multilayer films aimed at tissue engineering. *Soft Matter, 4*, 1422–1429.

Okushima, S., Nisisako, T., Torii, T., & Higuchi, T. (2004). Controlled production of monodisperse double emulsions by two-step droplet breakup in microfluidic devices. *Langmuir, 20*, 9905–9908.

Pancholi, K., Farook, U., Moaleji, R., Stride, E., & Edirisinghe, M. J. (2008a). Novel methods for preparing phospholipid coated microbubbles. *European Biophysics Journal, 37*, 515–520.

Pancholi, K., Stride, E., & Edirisinghe, M. J. (2008b). Generation of microbubbles for diagnostic and therapeutic applications using a novel device. *Journal of Drug Targeting, 16*, 494–501.

Pancholi, K., Stride, E., & Edirisinghe, M. J. (2008c). Dynamics of bubble formation in highly viscous liquids. *Langmuir, 24*, 4388–4393.

Stride, E., & Edirisinghe, M. J. (2008). Novel microbubble preparation technologies. *Soft Matter, 4*, 2350–2359.

Talu, E., Lozano, M. M., Powell, R. L., Dayton, P. A., & Longo, M. L. (2006). Long-term stability by lipid coating monodisperse microbubbles formed by a flow-focusing device. *Langmuir, 22*, 9487–9490.

Tan, W. H., & Takeuchi, S. (2007). Monodispers alginate hydrogel microbeads for cell encapsulation. *Advanced Materials, 19*, 2696–2701.

Wang, C. Y., Ye, S. Q., Dai, L., Liu, X. X., & Tong, Z. (2007). Enzymatic desorption of layer-by-layer assembled multilayer films and effects on the release of encapsulated indomethacin microcrystals. *Carbohydrate Research, 342*, 2237–2243.

Yang, J. S., Chen, S. B., & Fang, Y. (2009). Viscosity study of interactions between sodium alginate and CTAB in dilute solutions at different pH values. *Carbohydrate Polymers, 75*, 333–337.

Zhang, H. W., Cai, Q., Bei, J. Z., & Wang, S. G. (2004). The preparation of PLGA encapsulated Ca–alginate microspheres loaded with BSA and the release behavior of BSA. *Acta Polymerica Sinica, 454*, 457.